Proceedings of the Pakistan Academy of Sciences: A Physical and Computational Sciences 62(2): 149-164 (2025)

ISSN (Print): 2518-4245; ISSN (Online): 2518-4253
http://doi.org/10.53560/PPASA(62-2)879

Pakistan Academy of Sciences

Research Article

Granulometry based Extrapolation of Depositional Environment of Orangi Sandstone, Nari Formation Exposed around Hub Dam, Pakistan

Erum Bashir[1*], Sadia Khaleeq[2], Shahid Naseem[1], Maria Kaleem[1], Muhammad Shumail[2], and Wajih Ahmed[3]

[1]Department of Geology, University of Karachi, Karachi, Pakistan
[2]Department of Geology, Federal Urdu University of Arts, Science and Technology, Karachi, Pakistan
[3]Department of Geology, D.J. Sindh Govt. Science College, Karachi, Pakistan

Abstract: To infer the depositional environment, thirty-eight samples of the Orangi Sandstone-the uppermost unit of the Upper Oligocene Nari Formation, exposed at Hub Dam were collected. Granulometric data acquired from standard sieving techniques. The computed graphic mean's average value, was 1.38. Of the 38 samples, 24 were categorized as medium-grained, and the remaining 14 as coarse-grained. According to the sorting values, 36.84% of the samples were categorized as moderately sorted to moderately well-sorted, whereas 63.15% of the samples were poorly sorted. Skewness values showed a wide range from -2.17 to 2.65 suggesting a mixed population of coarse and fine skewed sediments. Kurtosis ranged from -2.46 to 2.97, showed situation of both leptokurtic and platykurtic. Bivariate plots created employing various textural parameters suggested predominantly fluvial origin with very few deviations. This interpretation is further supported by linear discriminant function analysis, which indicates a fluvial to shallow marine depositional setting for most samples. The study represents an initial attempt to appraise the vertical and lateral variability of the Orangi Sandstone using cement composition and textural parameters; skewness and kurtosis. The studied samples significantly reflect the impact of Upper Oligocene Period's tectonics, climate shift, and sea level fluctuations, and sediment transport dynamics. A model is constructed to describe the preponderant fluvial environment outlining the role of beach and tidal processes along with fluvial channels in the deposition of the sandstone.

Keywords: Granulometry, Depositional Model, Orangi Sandstone, Nari Formation, Hub Dam, Oligocene Age.

1. INTRODUCTION

Sandstones are formed by the lithification and cementation of sand-size particles [1]. Sandstones make up 10-20% of all rocks on the Earth and are extensively spread due to their tenacious character. Sandstones are significant from a variety of perspectives; they aid in comprehending the relief, topography, architecture, minerals, and chemical composition of any area; it is also beneficial for demonstrating the provenance and depositional patterns of a region [2-4]. In addition to being employed in construction and other industries [5], they host varieties of minerals [6], reservoirs of oil and gas [7] and are also serves as good aquifers too [8]. Inimitable genetic information and histories of depositional environments are naturally preserved in sandstones. Prime features that make up the texture of sandstone; particle size, sorting, and roundness are used to comprehend the conditions and processes that led to the deposition of the sediments [9]. To obtained textural parameters, granulometry is done by standard sieve analysis [2, 5]. The present study's region lies around Hub Dam, close to the Karachi trough. The Nari Formation (Oligocene to Early Miocene), which overlies the

Received: February 2025; Revised: May 2025; Accepted: June 2025
* Corresponding Author: Erum Bashir <ebahmed@yahoo.com>

Middle Eocene Kirthar Formation, is the oldest exposed formation [10]. The Nari Formation was formed in consequence of Himalayan orogeny, under tectonically unstable settings and underwent many periods of eustatic sea level changes. Five lithostratigraphic units are distinguished in the Nari Formation namely Orangi Sandstone is the youngest unit, followed by Pir Mangho, Halkani, Ghora Lakhi, and oldest Tobo unit respectively [8]. The Nari Formation's upper contact with the Gaj Formation is transitional and conformable [11].

Orangi Sandstone is the primary focus of the present study. This unit exhibits noticeable vertical and lateral facies variations, reflecting the dynamic interplay of tectonic activity, sediment supply, and marine transgressions during its deposition. The specific aims and objectives of this study are:

- To analyze the textural parameters (grain size, sorting, skewness, and kurtosis) of the Orangi Sandstone using statistical grain size analysis.
- To assess vertical and lateral facies variations in the study area and their relation to energy conditions and paleogeographic trends.
- To provide an interpretation of the depositional system, emphasizing the influence of hydrodynamic processes and tectonic settings during sedimentation.

By integrating grain size analysis with field observations of sedimentary structures like cross bedding, gradded bedding, ripple marks etc. and lithological variations, this research aims to enhance understanding of the paleodepositional settings and genetic evolution of the Orangi Sandstone within the broader framework of the Nari Formation. It may help to develop facies models in sedimentary basin analysis. This study may also assist for the reservoir quality prediction in hydrocarbons.

2. METHODOLOGY

2.1. Sample Collection

For the present study, 38 representative sandstone samples in a sequence from older to younger were collected from seven different sites. Considering the regional trend of the rocks, sampling was done from the outcrops of Orangi Sandstone exposed around and at the left bank of Hub Dam (Figure 1). Samples were collected in polyethylene bags to prevent loss of finer fractions, and then wrapped in towel to avoid physical damage during transportation to lab [12].

2.2. Sample Preparation

For size analysis, weakly cemented and friable sandstone samples were soaked in water, whereas the consolidated samples after crushing were soaked in 10% HCl solution for 24 hrs to remove cement from them [5]. Afterward, Whatman qualitative filter paper #1 was used to filter the sample. Using litmus paper, wash the sediment grains soaked in HCl many times until all the acid has been removed. First, the grains are adequately covered and dried at room temperature then in an electric oven. The samples were reduced in quantity and homogenized by applying coning and quartering method to obtain a representative sample [13].

2.3. Sample Analysis

Using a mechanical shaker (Model IL-60656 USA) and following the procedure described by [14], a 100-gram moisture-free sample was screened in an assembly of sieves (-1, 0, 1, 2, 3, 4 ϕ), pan and shaker. After shaking, each fraction was collected separately, weighed, and noted for further granulometry [15].

3. STUDY AREA

The research area is situated along the political border between Sindh and Balochistan provinces in the southwest of the Sindh Province. Its approximate boundaries are 25° 09′ to 25° 15′ N and 67° 02′ to 67° 12′ E (Figure 1); it's situated in the northwest of Karachi [16]. Tertiary rocks, particularly those from the Oligocene (Nari Formation) and Miocene (Gaj Formation) are exposed in the research area. These rocks were deposited over the Kirthar Formation due to the uplifting of the basin, after the Himalayan Orogeny [11].

The Nari Formation is deposited in two separate entities; the northern Nari Formation, which is exposed in the north of the study region from Dureji to Khuzdar, and the southern Nari Formation, which represents the Karachi Trough is exposed in the Lower Indus Basin [17]. Less thickness may be observed at the eastern and western edges of the Karachi Trough, whereas the northernmost portion has more thickness. The five

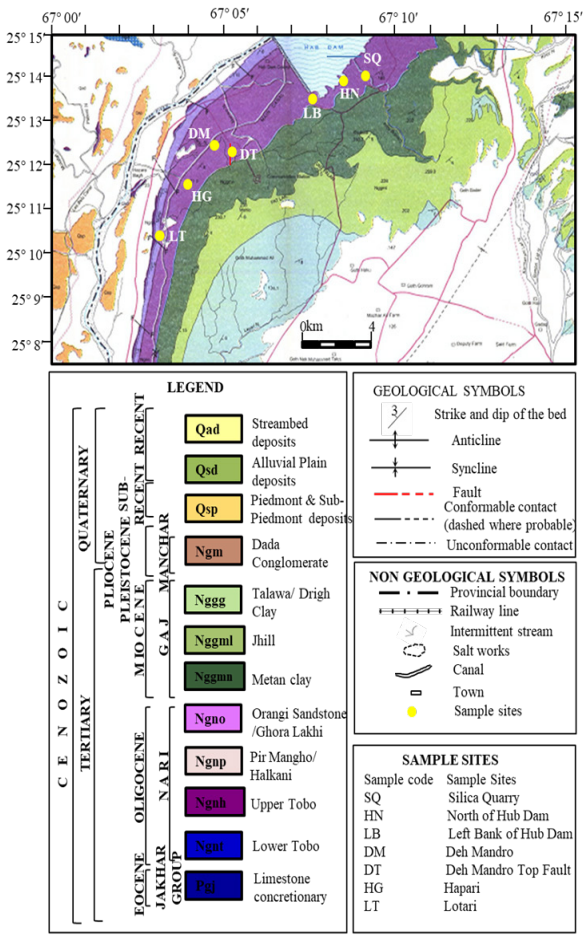

Fig. 1. Geological map of the study area showing sample sites, around Hub Dam after [16].

units of the Nari Formation include Tobo (oldest), Pir Mangho, Halkani, Ghora Lakhi, and youngest Orangi Sandstone [9, 16].

Orangi Sandstone is referred to as a variegated sequence due to the presence of yellow, brown, orange, violet, and red colours of cement; revealing the prevalence of varying levels of iron oxidation in the depositional system (Figure 2(a)). The siliceous cement is witnessed in the upper portion; it is often iron-free. Coarse-grained, even gritty layers are found at the top, whereas the bottom half is composed of fine-grained sandstone reflecting differences in the energy conditions of the depositional environment. Certain locations are extremely coarse grained and indicate channel depositional conditions. It has honeycomb structures, cross bedding, flute marks; grooves and ripple marks [18]. The Orangi Sandstone is devoid of fossils. There are also many neptunian dikes in some areas (Figure 2(b)).

Fig. 2. Field photographs showing: (a) colour variation in sandstone due to diversity of cement content, and (b) neptunian dyke in Orangi sandstone.

4. RESULTS

Table 1 displays the cumulative percentages of various fractions obtained from sieve analysis of studied samples. The weight percentages of the three main fractions (gravel, sand, and mud) of the samples are presented in Figure 3. Figure 4(a) displays general trends and location-wise sample cumulative curves of studied samples (Figure 4(b-h)). Most samples seem to be graded with varying degrees of gradation when compared to standard patterns. Table 2 and 3 exhibit calculated values, formulae, and categories of studied samples for the textural parameters. The graphic mean for the samples has an average value of 1.38 and a range of -0.02 to 2.72; while average value of standard deviation is 1.09 as mentioned in Table 2. Graphic skewness ranges between -2.17 to 2.65, with an average value of 0.10. Six of the Orangi Sandstone samples display strongly fine skewness, two show fine skewness, seven exhibits near symmetry, eight reveal coarse skewness, nine exhibit strongly coarse skewness, one sample has a value < -1.0, which appears as very strongly coarse skewed, and five samples have values > 1.0 and are classified as being very strongly fine skewed. The samples have a kurtosis range of -2.46 to 2.97, with a corresponding mean of 0.55. Table 3 displays 21 frequencies are extremely platykurtic, 4 platykurtic, 5 mesokurtic, 4 leptokurtic, and 4 very leptokurtic.

5. DISCUSSION

5.1. Granulometry

Granulometry is a popular method that is used to ascertain the depositional environment, origin, distribution, and transit of the rock [21, 22]. In addition, it offers crucial indications regarding the

Table 1. Sieve analysis data of studied samples and percentages of relatively coarse, medium and fine grain fractions.

	Cumulative Percentages after grain size analysis							Percentage of Fractions		
Sample Number	**-1**	**0**	**1**	**2**	**3**	**4**	**Finer**	**Gravel**	**Sand**	**Mud**
SQ4	5.02	10.09	15.46	20.80	53.30	77.08	100.00	5.02	72.06	22.92
SQ3	0.00	0.04	0.26	1.20	64.08	99.64	100.00	0.00	99.64	0.36
SQ2	0.00	0.00	0.50	2.76	67.64	99.20	100.00	0.00	99.20	0.80
SQ1	0.00	0.08	0.86	4.99	72.92	99.22	100.00	0.00	99.22	0.78
HN5	14.96	26.67	32.51	41.12	83.25	92.96	100.00	14.96	78.00	7.04
HN4	29.87	44.99	53.47	59.62	77.99	91.41	100.00	29.87	61.54	8.59
HN3	28.46	38.05	41.79	51.75	84.23	92.89	100.00	28.46	64.43	7.11
HN2	16.19	33.44	45.90	53.29	86.73	94.12	100.00	16.19	77.93	5.88
HN1	29.76	40.29	49.36	50.41	88.87	96.20	100.00	29.76	66.44	3.80
LB7	9.72	24.13	32.63	43.72	89.91	92.13	100.00	9.72	82.41	7.87
LB6	14.19	19.59	35.81	49.32	88.18	93.58	100.00	14.19	79.39	6.42
LB5	12.41	25.86	32.07	47.93	85.17	93.10	100.00	12.41	80.69	6.90
LB4	12.95	15.18	24.55	38.39	81.25	91.96	100.00	12.95	79.02	8.04
LB3	18.16	25.38	44.64	66.64	88.31	98.28	100.00	18.16	80.12	1.72
LB2	19.37	30.68	62.06	85.04	92.70	96.35	100.00	19.37	76.98	3.65
LB1	39.91	50.00	68.86	82.89	90.79	97.81	100.00	39.91	57.89	2.19
DM8	0.04	0.81	2.67	5.87	29.90	96.41	100.00	0.04	96.37	3.59
DM7	1.21	2.55	6.15	22.63	84.34	97.30	100.00	1.21	96.08	2.70
DM6	0.25	1.28	2.22	4.28	55.00	98.15	100.00	0.25	97.90	1.85
DM5	6.90	7.73	9.63	16.69	85.26	98.41	100.00	6.90	91.52	1.59
DM4	12.22	14.19	19.03	28.96	73.05	97.46	100.00	12.22	85.23	2.54
DM3	1.60	2.40	11.33	34.31	77.50	97.24	100.00	1.60	95.64	2.76
DM2	21.29	33.40	77.31	93.46	98.92	99.20	100.00	21.29	77.91	0.80
DM1	32.04	37.27	45.94	50.13	68.19	95.65	100.00	32.04	63.61	4.35
DT4	0.28	0.32	1.85	7.78	74.53	98.32	100.00	0.28	98.03	1.68
DT3	13.04	16.47	35.74	61.79	89.19	98.44	100.00	13.04	85.40	1.56
DT2	20.55	27.80	37.78	55.44	78.32	99.06	100.00	20.55	78.52	0.94
DT1	36.72	43.66	57.32	63.84	82.89	97.41	100.00	36.72	60.68	2.59
HG5	15.00	16.76	18.87	22.73	63.83	87.87	100.00	15.00	72.87	12.13
HG4	62.71	73.36	90.60	93.03	95.42	96.47	100.00	62.71	33.76	3.53
HG3	60.25	62.70	65.54	67.04	83.00	92.98	100.00	60.25	32.73	7.02
HG2	70.59	76.70	87.76	90.85	94.62	96.68	100.00	70.59	26.09	3.32
HG1	18.86	19.20	20.34	21.63	52.55	98.01	100.00	18.86	79.15	1.99
LT5	5.10	10.29	19.86	29.03	65.31	83.65	100.00	5.10	78.55	16.35
LT4	1.75	2.80	3.33	19.44	66.37	96.50	100.00	1.75	94.75	3.50
LT3	13.77	30.36	34.41	47.37	93.93	95.95	100.00	13.77	82.19	4.05
LT2	10.86	23.36	31.91	42.43	71.71	93.09	100.00	10.86	82.24	6.91
LT1	6.79	16.60	22.64	38.49	70.94	88.30	100.00	6.79	81.51	11.70

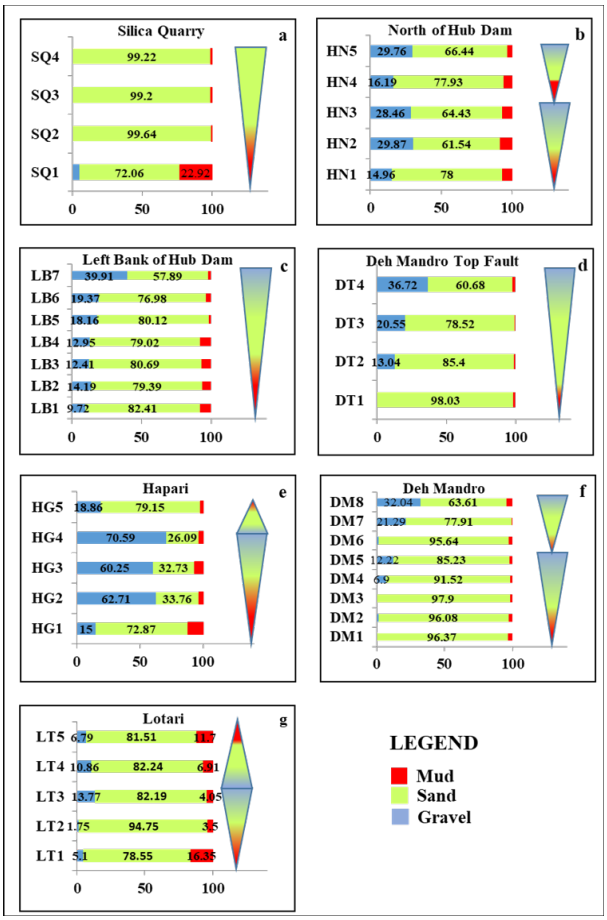

Fig. 3. Locality wise grain size fractions showing vertical distribution of grains (coarsening and finning sequences) and depositional cycles; fractions percentages are on x-axis and from bottom (older) to top (younger) samples are plotted on y-axis: (a) Silica Quarry, (b) North of Hub Dam, (c) Left Bank of Hub Dam, (d) Deh Mandro Top Fault, (e) Hapari, (f) Deh Mandro, and (g) Lotari.

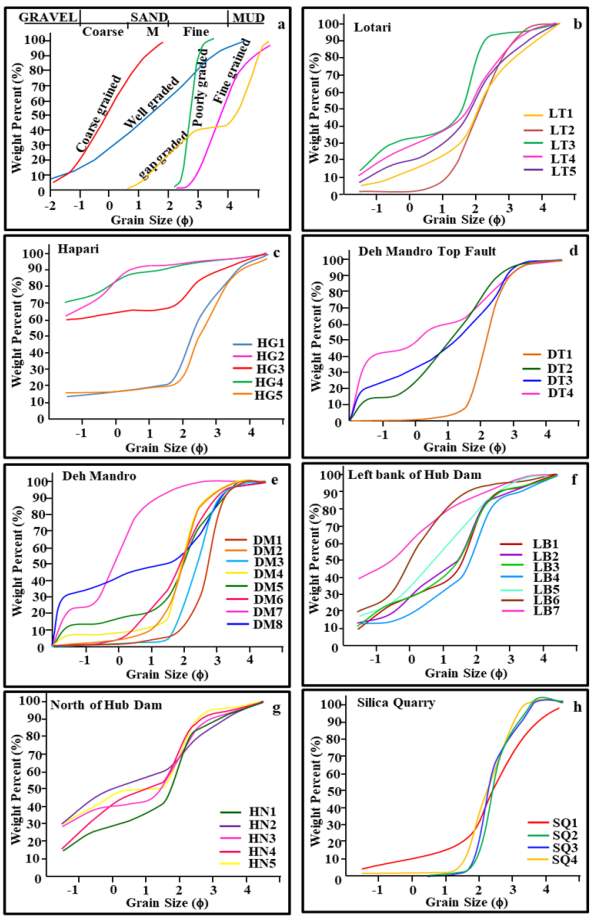

Fig. 4. Grain-size cumulative curves: (a) standard patterns, (b) Lotari, (c) Hapari, (d) Deh Mandro Top Fault, (e) Deh Mandro, (f) Left Bank of Hub Dam, (g) North of Hub Dam, and (h) Silica Quarry.

characteristics of sandstone reservoirs and the flow dynamics of systems [23]. Samples LT3, DT4, and DM7 (Figure 4(b, d-e)) exhibit curves resembling gap-graded pattern (Figure 4(a)); samples DT1, DM1-2 and 4 appear as poorly graded (Figure 4(d-e)). Sediment size grades provide important clues about the provenance and deposition of sediments [24]. Sand and gravel are coarse-grained sediments that are typically found in high-energy settings that can move larger particles, including rivers, near-shore zones, or areas that are impacted by waves or strong currents. Low-energy environments, such as deep lakes, estuaries, or offshore locations with weak currents, are associated with fine-grained sediments [25]. The sand was found to be the predominant component in the sieve analysis of the samples under study, followed by gravels (Figure 3). Only the SQ1 sample contains a significant percentage of fine-grained particles (i.e., 22.92%). The presence of a predominant coarse component in the examined samples suggests hydro-dynamically-driven deposition in rivers or near-shore settings.

5.2. Textural Parameters

For the textural study of sediments and depositional setting prediction, four key criteria are utilized: graphic mean size, sorting, skewness, and kurtosis. Folk [19] was the first to employ the graphic mean, which is the arithmetic average of the grain size in the sample. It shows the current velocity of the medium and turbulence in the deposition basin, together with the source's potential energy [25]. Amongst the 38 samples, twenty-four (63%) are medium-grained, and the remaining 37% samples are coarse-grained (Table 3). Overall, Orangi Sandstone samples are categorized as medium-grained. Such a grain pattern indicates that sandstone was formed under moderate to high energy conditions [26].

Table 2. Calculated values of textural parameters and classification of studied samples.

	Values				Classification			
Sample Number	**Mz**	**s_I**	**SKI**	**Kg**	**Mz**	**s_I**	**SKI**	**Kg**
SQ1	2.72	1.59	-0.08	1.51	Medium	ps	ns	vlk
SQ2	2.48	0.32	1.54	0.13	Medium	vws	vsfs	vpk
SQ3	2.45	0.39	1.41	0.16	Medium	ws	vsfs	vpk
SQ4	2.28	0.7	-0.05	00	Medium	mws	ns	vpk
HN1	1.7	1.56	-0.88	0.77	Medium	ps	scs	pk
HN2	0.22	1.55	1.21	0.32	Coarse	ps	vsfs	vpk
HN3	1.22	1.4	-0.96	0.28	Medium	ps	scs	vpk
HN4	0.83	1.46	-0.21	0.52	Coarse	ps	cs	vpk
HN5	0.72	1.36	-0.17	0.3	Coarse	ps	cs	vpk
LB1	1.4	1.08	-0.64	0.83	Medium	ps	scs	pk
LB2	0.95	1.38	-0.12	0.97	Coarse	ps	cs	mk
LB3	1.1	1.48	-0.27	1.42	Medium	ps	cs	lk
LB4	2.0	1.08	-0.84	1.35	Medium	ps	scs	lk
LB5	0.82	1.18	0.34	0.91	Coarse	ps	sfs	mk
LB6	0.37	0.78	0.87	0.43	Coarse	ms	sfs	vpk
LB7	0.35	0.83	1.49	0.51	Coarse	ms	vsfs	vpk
DM1	2.68	0.55	-0.34	1.87	Medium	mws	scs	vlk
DM2	1.93	0.39	-2.17	-2.46	Medium	ws	vscs	vpk
DM3	2.42	0.53	-0.02	0.87	Medium	mws	ns	pk
DM4	2.0	0.7	-0.72	2.97	Medium	mws	scs	vlk
DM5	1.42	1.49	-0.31	1.01	Medium	ps	scs	mk
DM6	1.85	1.03	-0.15	0.94	Medium	ps	cs	mk
DM7	-0.02	0.47	2.65	0.45	Coarse	ws	vsfs	vpk
DM8	1.52	1.27	0.03	0.52	Medium	ps	ns	vpk
DT1	2.25	0.53	0.14	1.2	Medium	mws	fs	lk
DT2	0.98	1.17	0.11	0.6	Coarse	ps	fs	vpk
DT3	0.65	1.59	-0.15	0.37	Coarse	ps	cs	vpk
DT4	0.2	1.61	0.53	0.35	Coarse	ps	sfs	vpk
HG1	2.5	1.08	-0.06	1.4	Medium	ps	ns	lk
HG2	0.02	0.54	1.0	-0.9	Coarse	mws	sfs	vpk
HG3	0.87	1.23	1.0	0.75	Coarse	ps	sfs	pk
HG4	0.07	0.6	1.0	-1.02	Coarse	mws	sfs	vpk
HG5	1.93	1.86	-0.77	0.6	Medium	ps	scs	vpk
LT1	1.92	1.45	-0.06	0.99	Medium	ps	ns	mk
LT2	2.16	0.99	-0.11	1.52	Medium	ms	cs	vlk
LT3	1.03	1.12	-0.32	0.42	Medium	ps	scs	vpk
LT4	1.33	1.59	-0.16	0.43	Medium	ps	cs	vpk
LT5	1.25	1.63	-0.09	0.65	Medium	ps	ns	vpk

Legend

ws	well sorted	ns	near symmetric	vpk	very platy kurtic
vws	very well sorted	vsfs	very strong finely skewed	vlk	very lepty kurtic
mws	moderately well sorted	vscs	very strong coarsely skewed	mk	meso kurtic
ms	moderately sorted	scs	strongly coarse skewed	lk	leptykurtic
ps	poorly sorted	sfs	strongly fine skewed	elk	extremely lepty kurtic
		cs	coarse skewed	pk	platy kurtic
		fs	finely skewed		

Sorting provides insights into the dependability of depositional and transportation processes. Better sorting will result from constant strength low or high currents, while poorly sorted sediments indicate mixed deposition and transportation [19]. Table 3 shows that the bulk of the samples (63%) are poorly sorted; 3 frequencies are classed as well sorted, 7 appear to be moderately well sorted, and

Table 3. Formulae, verbal limits and statistics of textural parameters [19, 20], and sample percentages.

Parameter/Class	**Formula/Range**	**No. of Studied Samples in each class**	**Values/ Percentage of Studied Samples**
Graphic Mean	Mz = (f16 + f50 + f84)/3	Minimum	-0.02
		Maximum	2.72
		Mean	1.38
Coarse grained	< 1	14	37%
Medium Grained	3-1	24	63%
Fine Grained	> 3	-	-
Inclusive Graphic Standard Deviation	$s_I = [(\phi_{84} - \phi_{16})]/4 + [(\phi_{95} - \phi_5)]/6.6$	Minimum	0.32
		Maximum	1.86
		Mean	1.09
Very well sorted	0.0 - 0.35	1	2.63%
Well sorted	0.35 - 0.50	3	7.89%
Moderately well sorted	0.50 - 0.71	7	18.42%
Moderately sorted	0.71 - 1.0	3	7.89%
Poorly sorted	1.0 - 2.0	24	63%
Very poorly sorted	2.0 - 4.0	-	-
Extremely poorly sorted	> 4	-	-
Inclusive graphic Skewness	$Sk_i = [(\phi16+\phi84-2\phi50)]/(2(\phi84-\phi16)] + [(\phi5+\phi95-2\phi50))/(2\ (\phi95-\phi5)]$	Minimum	-2.17
		Maximum	2.65
		Mean	0.1
Very strongly fine skewed	> +1	5	13.16%
Strongly fine skewed	+1.0 to +0.30	6	15.79%
Fine skewed	+0.30 to + 0.1	2	5.26%
Near symmetry	+0.10 to -0.10	7	18.42%
Coarse skewed	-0.10 to -0.30	8	21.05%
Strongly coarse skewed	-0.30 to -1.0	9	23.68%
Very strongly coarse skewed	< -1.0	1	2.63%
Graphic Kurtosis	$K_G = [(\phi95- \phi5)]/[2.44(\phi5 - \phi25)]$	Minimum	-2.46
		Maximum	2.97
		Mean	0.55
Very platykurtic	< 0.67	21	55.26%
Platykurtic	0.67- 0.90	4	10.53%
Mesokurtic	0.90 - 1.11	5	13.16%
Leptokurtic	1.11 - 1.50	4	10.53%
Very leptokurtic	1.50 - 3.0	4	10.53%
Extremely leptokurtic	> 3.0	-	-

where ϕ_5, ϕ_{16}, ϕ_{25}, ϕ_{50}, ϕ_{75}, ϕ_{84} and ϕ_{95} represents 5^{th}, 16^{th}, 25^{th}, 50^{th}, 75^{th}, 84^{th} and 95^{th} percentiles respectively on the cumulative curve.

3 samples are moderately sorted. It may be due to the rapid forth and backflow of the depositional environment as suggested by [27]. Poor sorting in sandstone is a sign that the basin contains variable-size sediments that may have been deposited by turbulent flow and currents with different velocities [28]. Present work also get support from the study of Kasim *et al*. [29] while working on onshore Peninsular Malaysia; showed that short-distance movement and deposition in a river environment are reflected by the predominance of poorly sorted sediments.

An imbalance in the grain size distribution curve is called skewness. According to Azidane *et al*. [30], skewness is a nuanced metric that may be used to assess subpopulation mixing and the energy circumstances that prevailed during deposition. Around 47% of samples have positive skewness values, followed by 34% with negative values and 18% with almost symmetrical values, which indicate mixing of the deposition and transit circumstances. Negatively skewed sediments are deposited because of high energy conditions, while symmetrically skewed sediments will thrive in low-intensity environments [31]. Mir and Jeelani [32] stated that positive skewness indicates unidirectional transportation and the deposition of sediments in low-energy settings. Additionally, Kasim *et al*. [29] reported that positive skewness in sediments is a result of fluvial settings. Most of the examined samples appear to originate from the fluvial environment, according to skewness and other textural metrics taken together. The degree of peakedness in the grain size distribution is known as graphic kurtosis [33-34]. According to Boboye *et al*. [22], it is a measure of the ratio between sorting the graph's center and tail. The mean values of studied samples reflect a preponderance of platykurtic character. Large variation in the values of kurtosis can be attributed to the fluctuation in depositional currents [35].

5.3. Environmental Interpretation

5.3.1. Bivariate analysis

By integrating several grain size factors in bivariate plots, one may reduce possible ambiguities associated with individual proxies and provide a more inclusive understanding of the paleo-environment/ paleo-provenance [36-37]. Additionally, it may be applied to distinguish between different sedimentation settings and analyze energy circumstances [30]. To interpret the paleo-environment based on sedimentological constraints, a few scatter plots were made, including mean vs. standard deviation [26], mean vs. skewness, sorting vs. skewness [27], and Stewart diagram [30].

To understand the origin of sediment, Ayodele and Madukwe [27] employed a bivariate visualization between sorting and mean grain size that showed the analyzed samples were deposited by fluvial processes (Figure 5(a)). The Figure 5(b), which distinguishes between overbank, river channel, and overbank-pool deposits, illustrates that majority of the samples are inclined towards river channel deposits. Using the same granulometric metrics, Elsherif *et al*. [34]; and Moiola and Weiser [38] also demarcated the fields of beach, coastal dune, and river-deposited sediments. Few samples diverged towards the coastal dune to beach habitat, while majority of the samples seemed to have been deposited by rivers (Figure 5(b)).

Mean sizes against skewness plots are another tool used by Ayodele and Madukwe [27] to identify overbank and overbank-pool as well as river channel deposits. Most of the examined samples are plotted around the deposits seen in river channels (Figure 6(a)). The above-stated outcome is further corroborated by research of Folk and Ward [20], Adeoye *et al*. [39], and Kasim *et al*. [29], who divide beach/near shore, tidal current and fluvial environment using a customized plot of skewness vs. standard deviation (sorting). Plots of the samples on skewness vs. standard deviation bivariate graph show that 71% of them are inside the river zone, suggesting that the samples were

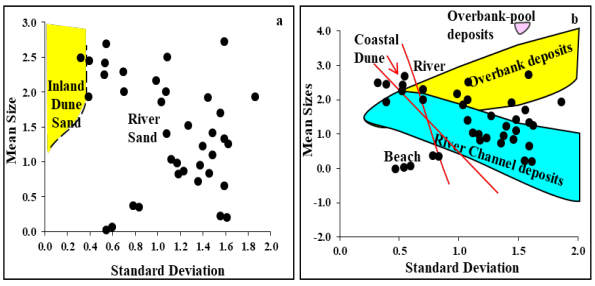

Fig. 5. Scattered plots between mean size and standard deviation reflecting: (a) nature of sediments after [27] and (b) type of deposits after [38]; while boundaries marked by red lines after [34].

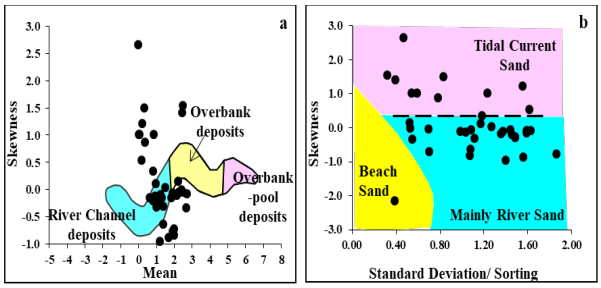

Fig. 6. Bivariate plots between: (a) mean vs. skewness after [27], and (b) standard deviation vs. skewness after [39].

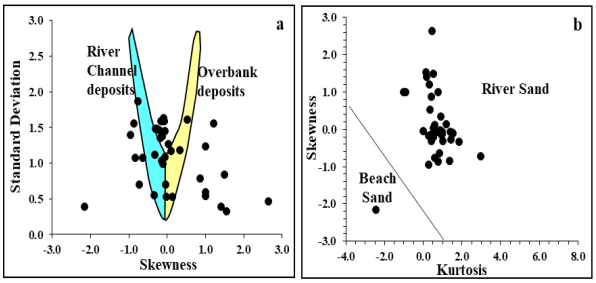

Fig. 7. Scattered plots between: (a) skewness vs. standard deviation after [27], and (b) Kurtosis and Skewness after [39].

transported and deposited by rivers (Figure 6(b)). In contrast, 23% of samples diverged and were deposited by tidal currents.

Furthermore, it is reinforced by research conducted by Ayodele and Madukwe [27], which used a graph between sorting and skewness to distinguish between overbank deposits and river channel fields. Although the plots of the analyzed samples are rather dispersed, most of them are oriented towards river deposits (Figure 7(a)). Adeoye *et al*. [39] distinguished between river and beach sands using a kurtosis vs. skewness plot. The fluvial provenance of sandstones is validated by the bivariate graph in Figure 7(b) that shows the dominance of river transportation between kurtosis and skewness of the studied samples.

5.3.2. Linear discriminant function (LDF)

A powerful method for determining the predominant sedimentation process in the area is Sahu's linear discriminant function, which was employed by several studies [29, 40]. Sahu [41] made use of statistical measures and constituted four LDFs (Y1, Y2, Y3, and Y4) to construe the energy and fluidity of depositional environments. Equations for LDFs, their ranges, interpretation of the deposition environment, and the estimated values of analyzed samples are shown in Table 4. About 76% of samples appear to have Y1 values > -2.7411, indicating a beach environment while nine samples have values less than -2.7411, indicating a tendency towards an aeolian environment of deposition. More than 92% of the samples reveal deposition in a shallow, turbulent marine environment, having a value of Y2 > 65.3650. Only three samples were recognized by the discriminant Y2 as deposits from the beach environment. When accounting for Y3, 100% of the samples had values less than -7.419 which indicates a fluvial environment. Mutual deposition in turbid and fluvial settings is implied by the Y4 values; 52.6% of the samples have values less than, and 47.4% of samples have values greater than -2.7411 (Table 4). The average values of all LDFs collectively, for all samples show shallow water to fluvial environment with minimal turbidity current effect.

The cross-plots Y2 vs. Y3 (Figure 8(a)) and Y3 versus Y4 (Figure 8(b)) are designed to verify the actual conditions that existed during the deposition of Orangi Sandstone. It was most likely deposited in the transitional zone under the combined effect of fluvial and shallow agitated water conditions, according to the bivariate plots. The worldwide eustatic curve pattern which shows constant variations in sea level throughout the Oligocene, lends more credence to this assumption. According to Welcomme *et al*. [45], the Nari Formation in the southernmost Kirthar Province is composed of well-developed transgressive marine sediments that were gradationally influenced by river circumstances.

5.3.3. Stewart diagram

Stewart [43] presented a graphical representation

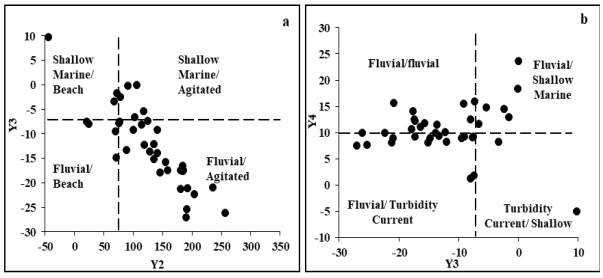

Fig. 8. Discrimination of environment of studied samples based on LDF plots: (a) Y2 vs. Y3 after [40], and (b) Y3 vs. Y4 after [29].

Table 4. Linear discriminate functions (LDF) formulae for calculation after Sahu [41] and environmental interpretation after [27].

Linear Discriminate Function	Environment	Formulae	Interpretation	Studied Samples
Y1	Aeolian and Beach	Y1 = −3.5688 Mz + 3.7016 σ_i^2 − 2.0766 SK + 3.1135 KG	Y1 < −2.7411 represents Aeolian deposition; Y1 > −2.7411 signifies Beach environment	Min. -11.2798 Max. 9.44 Mean 1.95 Aeolian 23.68% Beach 76.32%
Y2	Beach and Shallow Agitated Marine	Y2 = 15.6534 Mz + 65.7091 σ_i^2 +18.1071 SK +18.5043 KG	Y2 < 65.3650 indicates Beach deposition; Y2 > 65.3650 represents Shallow Agitated Marine environment	Min. -44.4302 Max. 255.87 Mean 126.10 Beach 7.89% Shallow Agitated Marine 92.11%
Y3	Shallow Agitated Marine and Fluvial	Y3 = 0.2852 Mz −8.7604 σ_i^2 − 4.8932 SK1+ 0.0482 KG	Y3 < −7.419 characterize Fluvial environment; Y3 > −7.419 the environment is Shallow Marine.	Min. -27.0356 Max. 9.696 Mean -12.1759 Fluvial 100%
Y4	Fluvial and Turbidity Conditions	Y4 = 0.7215 Mz + 0.403 σ_i^2 + 6.7322 SK + 5.2927 KG	Y4 < 10.000 the environment is Fluvial and if >10.000, the environment is Turbidity	Min. -4.9493 Max. 23.7029 Mean 10.5007 Fluvial 52.64% Turbidity 47.36%

of depositional processes utilizing median grain size and sorting in phi values. Three processes that reflect distinct sedimentary settings explained by the Stewart diagram are: (1) wave action-driven shoreward processes; (2) fluvial events, especially floods; and (3) slow deposition from calm seas. Lukman *et al*. [44] and Parthasarathy *et al*. [45] further revised it and demarcated the inner shelf environment on the Stewart diagram. Samples plotted on the Stewart diagram reveal that river activities had a major influence on the Orangi Sandstone, with wave action having a combined effect on a small number of samples (Figure 9). This behavior suggests that the Orangi Sandstone may have been deposited in a transitional environment.

5.3.4. Vertical-Lateral variation in studied samples

The exposition of depositional environment depends on studies of lateral and vertical variation in rock assemblage [46]. These differences may primarily be described for sedimentological investigations based on the lithology, grain size, colour, bed continuity, and primary structures. Sandstone was found to be the predominant lithology in the samples under study, followed by conglomerates.

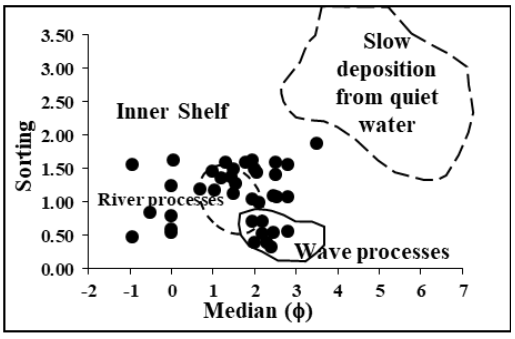

Fig. 9. Plots of studied samples on Stewart diagram [43] based on sorting and median values; boundaries after [30].

Additionally, variations in sandstone were observed, with the most common types being pure sandstone, muddy sandstone, gravelly sandstone; and just six samples make up the sandy conglomerate facies (see Figure 10).

The lithology's spatial distribution pattern (Figure 11) shows that in the extreme northeast (the Silica quarry site), the predominant facies is pure sandstone, while the amount of gravel and mud rises as one moves towards west (to the HN and LB). Little mud and coarse fraction of sandstone are present in the early stages of deposition; however, as time goes on, the amount of gravel in the strata rises steadily, causing the facies to transition from muddy gravelly sandstone to gravelly sandstone to sandy conglomerate. The repetition of facies in vertical succession is observed in the Lotari (LT) and Hapari (HG) sites in the southwest (Figure 3). Comparison of the locality-wise distribution of grain size (Figure 3) shows that there are two depositional sequences in southwest localities (LT and HG), from older to younger samples. In bottom samples, a coarsening upward pattern is observed, followed by a finning upward pattern in top samples that complies with Walther's law of facies. The existence of sole marks and the normal grading of sediments (upward finning) indicate that turbidity currents are responsible for deposition. Similar circumstances were also mentioned by Zou *et al.* [48] during their investigation of the Yanchang Formation in China. The samples taken from the north of Hub Dam (HN) and Deh Mandro (DM) sites showed two cycles of deposition. In each cycle, upward coarsening sequences were observed; in contrast, only one upward coarsening cycle was witnessed at the sites of DT, LB, and SQ (Figure 1). Hiatt [49] states that fining upward sedimentary facies successions are symbolic of point bar deposits (i.e., banks of meander bends) in the fluvial environment, while coarsening upward facies successions are suggestive of prograding shoreface and deltaic environments.

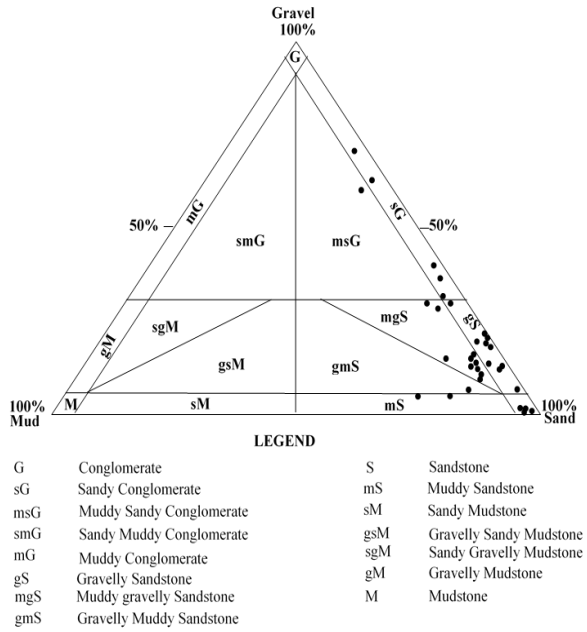

Fig. 10. Classification of studied samples on sand-gravel-mud diagram, fields after [47].

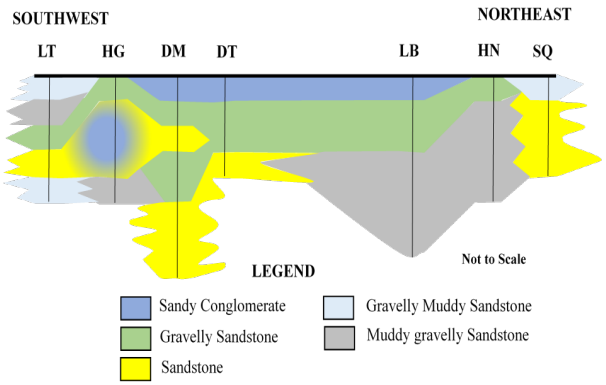

Fig. 11. Lateral variation in lithology of studied samples from southwest to northeast.

The primary ingredient that binds the sediments to create a consolidated rock is cement. This can indicate the depositional site's oxidation conditions and can originate from several sources during diagenesis. Cementing material's spatial distribution exhibits vertico-lateral variation within the samples (Figure 12(a)). Three different forms of cement are found in the samples under study, ranging in composition from calcareous, ferruginous to siliceous in varying proportions. Deposits of ferruginous material occur in conditions of high (hematite) to somewhat low (limonite) oxidation. The occurrence of iron oxide; hematite cement in the bottom samples and limonite in the top samples of the LT section (Figure 12(a)), indicates an oscillating environment that is also evident in the lithology and grain size. Towards NE, the ferrous material was altered to ferric oxide with the addition of calcareous cement. The calcareous cement samples are comparatively harder. The small-scale syn-depositional fault is the cause of the calcareous cement observed in the HG2-HG4 samples (Figure 12(a)). The distribution and content of cement are

ultimately influenced by fractures and faults, which control the fluid movement across stratigraphic units [50]. Sample HG5 and SQ1 contain siliceous cementing material; the latter (SQ1) is collected from silica quarry. The reason for the low siliceous cement in other samples is that in the fluvial environment, shallow meteoric water produces very little siliceous content [51].

For the first time, textural factors (kurtosis and skewness) are utilized in addition to lithology and cementing material to create lateral variation within the Orangi Sandstone. Based on kurtosis analysis (Figure 12(b)), most samples exhibit very platykurtic distributions, indicating a wide spread in grain size and suggesting poor sediment sorting. When integrated with lithological characteristics and grain size data, this facies is divided into two: Subfacies-1with relatively coarse grains and a gritty texture found on top, whereas subfacies-2, located below the top, have a texture with medium sand grains. The platykurtic facies are mostly found in the lower sedimentary successions, indicating that they were deposited under conditions of rapid, erratic flow, perhaps as a result of abrupt sediment influx. Conversely, mesokurtic to very leptokurtic facies predominate in the central parts of the successions, especially those that trend southwestward. These are typically linked to fine to very fine-grained, poorly sorted sandstones, which are a sign of high-energy settings like swift-moving river systems that can carry finer sediments in suspension and deposit them selectively when energy levels are dropping [52]. These deposits' leptokurtic character indicates more consistent flow dynamics during deposition and reflects a narrower grain size distribution. Figure 12(c) shows the distribution of the skewness of studied samples. There are two distinct facies identified: the strongly to very strongly fine skewed and the coarse to strongly coarse skewed facies. For most of the research area, both facies are found parallel to one another (Figure 12(c)), indicating a fluctuating environment. On the other hand, symmetrical to very fine skewed facies predominate in the northeast site (SQ), whereas coarse skewed facies dominate at the extreme southwest site.

5.4. Depositional Model

A complete picture of the depositional basin and related geodynamic environment may be obtained from the variation in grain size, the difference in facies, and the variety of cementing materials in a clastic sequence [49]. In the fluvial-deltaic system of deposition, the vertico-lateral variation offers insights into flow regimes [31]. The tectonic system of an area is crucial in generating facies heterogeneity [53]. The Early Tertiary India-Eurasia convergence had effects on the research region [54]. Variations in sea level at the time of

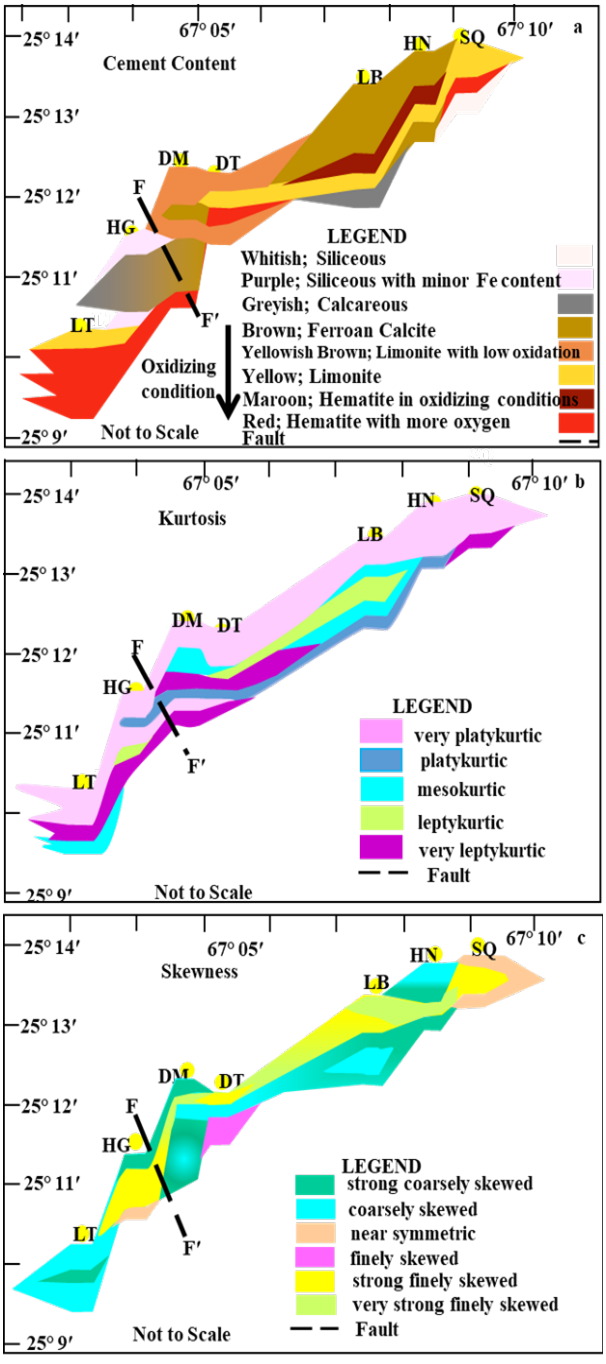

Fig. 12. Idiosyncrasy of studied samples based on variations in: (a) cement content, (b) kurtosis values, and (c) skewness values.

deposition also contribute to the supply of sediment [55]. An integrated approach is used to create a schematic depositional model below.

The Indian Plate had a major tectonic event near the end of the Cretaceous (65 Ma) when it crossed over the Réunion hotspot. This caused the Proterozoic Aravalli igneous and metamorphic complex to erode. According to Mehmood *et al*. [46], the weathered sediments were deposited as the Maastrichtian Pab Formation in the southern Indus Basin. Based on paleocurrent data and discrimination diagrams, Ahmed *et al*. [18] and Umar *et al.* [56] demonstrated that the sediments of the Pab Sandstone originated from the Precambrian Aravali Mountain belt, which is in the east and southeast along the boundary between Pakistan and India.

The deposition of the Nari and Gaj formations as well as the Siwaliks was caused by three different periods of sediment supply, which Kazmi and Jan [57] categorized from north to south. These stages are the Middle to Late Paleocene, Early Oligocene to Early Miocene, and Middle Pliocene to Pleistocene. Throughout the Cenozoic era, there were variations in the deposition of sediments in a variety of locations, mostly because of sea level oscillations. These changes included rising (Himalayan orogeny), erosion, and subsequent deposition. The sea receded southward until the Oligocene (40 Ma), when it formed shallow marine depositional basins in the Karachi region, mostly in the form of estuaries and embayments [58]. Sea level rise from 27 to 23 Ma was constant in the Orangi Sandstone unit of the Nari Formation, from 130 to 160 meters. The deposition of Orangi Sandstone in the variable environment is also reflected in the interpretation of grain size textural factors.

Keeping this in mind, a fabricated depositional model of the Orangi Sandstone in the research region is shown Figure 13. This model also gets support from the study Paryal *et al.* [59] and Samtio *et al.* [35] who also confirmed that the Nari Formation was deposited in a shallow marine basin, mostly as a beach and deltaic environment while working in the Kirthar Province.

This diagram depicts a thorough depositional model moving from continental to deep marine

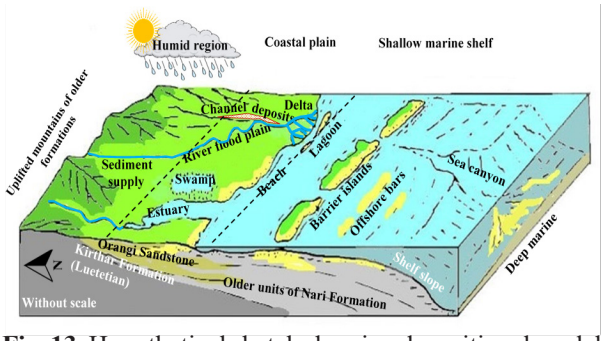

Fig. 13. Hypothetical sketch showing depositional model of Orangi Sandstone in the study area during Oligocene, marked by broken lines.

environments revealing the deposition of various units of Nari Formation. Uplifted mountainous areas with a humid climate are the source of sediments, which causes severe weathering and erosion. These sediments eventually form deltaic deposits along the coast after being carried by a fluvial system that includes river flood plains, swamps, estuaries, and channel deposits. The Orangi Sandstone is stratigraphically positioned above older Nari Formation units, indicating a transgressive-regressive depositional history impacted by tectonic activity and variations in sea level. It is also supported by presence of cross-bedding and ripple marks reflecting river or tidal channel activity. Further, occurrence of honeycomb weathering suggests chemical weathering in a marine or tidal setting under humid or semi-arid conditions. The processes of sediment dispersal and facies variation throughout a foreland are well represented by this model. This model effectively captures the facies variation and sediment dispersal processes across a foreland basin system.

6. CONCLUSIONS

Based on lithology, grain size, and cementing material it is concluded that Orangi Sandstone is a pure sandstone that reflects medium to coarse-grain size sand particles. The sandstone exhibits gravelly to sandy-muddy texture with few exceptions. The presence of all three types of cement (calcareous, ferruginous, and siliceous) reveals the deposition of Orangi sandstone under variable flow conditions. The sedimentological statistics also certified the transitional fluctuating depositional environment. The extremely platykurtic to platykurtic-type facies are dominated and are mostly found in the upper parts of the studied section while the

mesokurtic to leptokurtic facies are restricted to the southwest sections and are enclosed by extremely platykurtic to platykurtic-type facies. The pattern of kurtosis and simultaneous occurrence of coarse to extremely coarse and strong to very strongly fine skewed facies supports the deposition of Orangi Sandstone in the shallow marine to fluvial-deltaic zone, where the channel, tidal current, and beach/near coast environment existed. Conceptual model of deposition exhibited that accumulation of the Orangi Sandstone has occurred over older Nari Formation units, with sediments being transported from the uplifted northern terrain into the depositional basin. The model invokes an Upper Oligocene tectonic uplift, tied to Himalayan orogenic activity, and associated sea-level rise and fall, leading to fluctuating energy conditions and sedimentation patterns.

7. CONFLICT OF INTEREST

The authors declare no conflict of interest.

8. REFERENCES

1. D. Liu, Z. Gu, R. Liang, J. Su, D. Ren, B. Chen, and C. Yang. Impacts of pore-throat system on fractal characterization of tight sandstones. *Geofluid* 2020(1): 4941501 (2020).
2. J.E. Houghton, J. Behnsen, R.A. Duller, T.E. Nichols, and R.H. Worden. Particle size analysis: A comparison of laboratory-based techniques and their application to geoscience. *Sedimentary Geology* 464: 106607 (2024).
3. R. Khalil. Investigating the depositional environments using particle-size analysis of Lower Cretaceous sandstone reservoirs, Biyadh Formation, Saudi Arabia. *Journal of Taibah University for Science* 18(1): 1-9 (2024).
4. C.A. Allen, I.G. Udo, T.A. Harry, and A.E. Ekot. Granulometric and Pebble Morphometric Analyses of Sandstone Lithofacies of the Ameki Formation in Northeastern Part of Akwa Ibom State, Niger Delta, Nigeria. *Researchers Journal of Science and Technology* 4(1): 32-44 (2024).
5. A. Khan, U. Khadim, and S. Anjum. Assessment of Orangi Sandstone Unit of Nari Formation, Karachi: Industrial Applications with Special Focus on Glass Making. *International Journal of Ground Sediment & Water* 7 (1): 365-380 (2018).
6. G. Wang, Q. Lei, Z. Huang, G. Liu, Y. Fu, N. Li, and J. Liu. Genetic Relationship between Mississippi Valley-Type Pb–Zn Mineralization and Hydrocarbon Accumulation in the Wusihe Deposits, Southwestern Margin of the Sichuan Basin, China. *Minerals* 12(11): 1447 (2022).
7. R.M. Abraham-A, F. Taioli, and A.I. Nzekwu. Physical properties of sandstone reservoirs: Implication for fluid mobility. *Energy Geoscience* 3(4): 349-359 (2022).
8. M.T. Sohail, A. Hussan, M. Ehsan, N. Al-Ansari, M.M. Akhter, Z. Manzoor, and A. Elbeltagi. Groundwater budgeting of Nari and Gaj formations and groundwater mapping of Karachi, Pakistan. *Applied Water Science* 12(12): 267 (2022).
9. Y. Yan, L. Zhang, X. Luo, K. Liu, B. Yang, and T. Jia. Simulation of ductile grain deformation and the porosity loss predicted model of sandstone during compaction based on grain packing texture. *Journal of Petroleum Science and Engineering* 208 (1): 109583 (2022).
10. N.K. Siddiqui (Ed.). Petroleum Geology, Basin Architecture and Stratigraphy of Pakistan. *Nusrat K. Siddiqui* (2016).
11. S.M.I. Shah. Stratigraphy of Pakistan. Volume 22. *Geological Survey of Pakistan* (2009). https://hostnezt.com/cssfiles/geology/STRATIGRAPHY%20OF%20PAKISTAN%20BY%20S.M.%20IBRAHIM%20SHAH.pdf
12. G. Li, C. Qi, Y. Sun, X. Tang, and B. Hou. Experimental Study on the Softening Characteristics of Sandstone and Mudstone in Relation to Moisture Content. *Shock and Vibration* 14(1): 4010376 (2017).
13. J. Alali. Mineral Processing of Silica Sand in Hanout Area South of Jordan. *Open Journal of Geology* 13(7): 667-696 (2023).
14. C. Zoramthara, V.Z. Ralte, and Lalramdina. Grain-size analysis of Tipam sandstones near Buhchang village, Kolasib district, Mizoram. *Science Vision* 15(Supplementary issue): 43-51 (2015).
15. R. Khalil. Grain-Size Analysis of Middle Cretaceous Sandstone Reservoirs, the Wasia Formation, Riyadh Province, Saudi Arabia. *Sustainability 15*(10): 7983 (2023).
16. S.A. Khan, Z. Saeed, A. Khan, G. Hamid, and S.W. Haider. Assessment of Soil Liquefaction Potential in Defence Housing Authority, Karachi, Pakistan. *International Journal of Economic and Environmental Geology* 8(2): 63-68 (2017).
17. I.B. Kadri (Ed.). Petroleum Geology of Pakistan. *Pakistan Petroleum Limited* (1995).
18. Z. Ahmed, A. Khan, and B. Ahmed. Sandstone Composition and Provenance of the Nari Formation,

Central Kirthar Fold belt, Pakistan. *Pakistan Journal of Geology* 4(2): 90-96 (2020).
19. R.L. Folk (Ed.). Petrology of Sedimentary Rocks. *Austin, Hemphill Publishing Company* (1956).
20. R.L. Folk and W.C. Ward. Brazos River Bar: A Study in the Significance of Grain Size Parameters. *Journal of Sedimentary Research* 27(1): 3-26 (1975).
21. Y. Shi, E. Chongyi, Z. Zhang, Q. Peng, J. Zhang, W. Yan, and C. Xu. Comparison and significance of grain size parameters of the Menyuan loess calculated using different methods. *Open Geosciences* 15(1): 20220474 (2023).
22. O.A. Boboye, O.K. Jaiyeoba, and E.E Okon. Characteristics and mineralogical studies of some Cretaceous sandstones in Nigeria: implications for depositional environment and provenance. *Journal of sedimentary Environments* 6(4): 531-550 (2021).
23. H.L. Brooks, E. Steel, and M. Moore. Grain Size Analysis of Ancient Deep-Marine Sediments using Laser Diffraction. *Frontiers in Earth Science* 10: 820866 (2022).
24. G. Li, R. Du, J. Tang, Z. Li, Q. Xia, B. Shi, L. Zhou, Y. Yang, and W. Zhang. Comparison of the graphic and moment methods for analyzing grain-size distributions: A case study for the Chinese inner continental shelf seas. *International Journal of Sediment Research* 37(6): 729-736 (2022).
25. M. Roem, M. Musa, and Y. Risjani. Sediment dynamics and depositional environment on Panjang Island reef flat, Indonesia: insight from grain size parameters. *Aquaculture, Aquarium, Conservation & Legislation* 14(1): 357-370 (2021).
26. G.O. Aigbadon, A. Ocheli, O.C. Akakuru, E.O. Akudo, S.D. Christopher, O. Esharive, and J.A Francis, Paleoenvironments and hydrocarbon reservoir potentials from the selected sedimentary basins in Nigeria using sedimentary facies and textural analyses. *Journal of Sedimentary Environments* 7 (3): 371-401(2022).
27. O.S. Ayodele and H.Y. Madukwe. Granulometric and Sedimentologic Study of Beach Sediments, Lagos, Southwestern Nigeria. *International Journal of Geosciences* 10(3): 295-316 (2019).
28. A.D. Miall (Ed.). The geology of fluvial deposits: Sedimentary facies, basin analysis and petroleum geology. *Springer* (1996).
29. S.A. Kasim, M.S. Ismail, and N. Ahmed. Grain size statistics and morphometric analysis of Kluang-Niyor, Layang-Layang, and Kampung Durian Chondong Tertiary Sediments, Onshore Peninsular Malaysia: Implications for paleoenvironment and depositional processes. *Journal of King Saud University-Science* 35(2): 102481 (2023).
30. H. Azidane, B. Michel, M.E. Bouhaddioui, S. Haddout, B. Magrane, and A. Benmohammadi. Grain size analysis and characterization of sedimentary environment along the Atlantic Coast, Kenitra (Morocco). *Marine Georesources & Geotechnology* 39(5): 569-576 (2021).
31. T.J. Arun, K.R. Prasad, T.D. Aneesh, A.T. Limisha, M.K. Sreeraj, and R. Srinivas. Studies on the Textural Characteristics of Sediments from Periyar River Basin, Kerala, Southern India. *International Journal of Applied Environmental Sciences* 14(5): 495-526 (2019).
32. R.A. Mir and G.H. Jeelani. Textural characteristics of sediments and weathering in the Jhelum River basin located in Kashmir Valley, western Himalaya. *Journal of the Geological Society of India* 86: 445-458 (2015).
33. R.L. Folk. A review of grain-size parameters. *Sedimentology* 6(2): 73-93 (1966).
34. E.A. Elsherif, A. Badawi, and T. Abdelkader. Grain size distribution and environmental implications of Rosetta beach, Mediterranean Sea coast, Egypt. *Egyptian Journal of Aquatic Biology & Fisheries* 24(1): 349-370 (2020).
35. M.S. Samtio, A.A.A.D. Hakro, R.A. Lashahri, A.S. Mastoi, R.H. Rajper, and M.H. Agheem. Depositional Environment of Nari Formation from Lal Bagh Section of Sehwan Area, Sindh Pakistan. *Sindh University Research Journal* 53(01): 67-76 (2021).
36. Q. Zhang, Y. Wang, X. Wang, H. Yang, and T. Wang. Grain-size characteristics and sedimentary environmental significance of terrestrial red sandstone in the Dongying Depression with a gentle slope zone. *Bulletin of Geological Science and Technology* 43(5): 81-94 (2024).
37. S. Mishra, R.N. Hota, and B. Nayak. Grain size analysis and an overview of the sedimentary processes in Chandrabhaga beach, east coast of India. *Arabian Journal of Geosciences* 17(7): 214 (2024).
38. R.J. Moiola and D. Weiser. Textural parameters; an evaluation. *Journal of Sedimentary Research* 38(1): 45-53 (1968).
39. J.A. Adeoye, V.O. Jolayemi, and S.O. Akande. Sedimentology and foraminiferal paleoecology of the exposed Oligocene–Miocene Ogwashi-Asaba Formation in Issele-Uku area, Anambra Basin, southern Nigeria: A paleoenvironmental reconstruction. *Journal of Palaeogeography* 11(4):

618-628 (2022).

40. C. Baiyegunhi, K. Liu, and O. Gwavava. Grain size statistics and depositional pattern of the Ecca Group sandstones, Karoo Supergroup in the Eastern Cape Province, South Africa. *Open Geosciences* 9(1): 554-576 (2017).
41. B.K. Sahu. Depositional Mechanisms Form the Size Analysis of Clastic Sediments. *Journal of Sedimentary Petrology* 34 (1): 73-83 (1964).
42. J.L. Welcomme, M. Benammi, J.Y. Crochet, L. Marivaux, G. Métais, P.O Antoine, and I. Baloch. Himalayan Forelands: palaeontological evidence for Oligocene detrital deposits in the Bugti Hills (Balochistan, Pakistan). *Geological Magazine* 138 (4): 397-405 (2001).
43. H.B. Stewart. Sedimentary Reflections of Depositional Environments in San Miguel Lagoon, Baja California, Mexico. *American Association of Petroleum Geologists Bulletin* 42(11): 2567-2618 (1958).
44. A.M. Lukman, R. Ayuba, and T.S. Alege. Sedimentology and depositional environments of the Maastrichtian Mamu Formation, Northern Anambra Basin, Nigeria. *Advances in Applied Science Research* 9(2): 53-68 (2018).
45. P. Parthasarathy, G. Ramesh, S. Ramasamy, T. Arumugam, P. Govindaraj, S. Narayanan, and G. Jeyabal. Sediment dynamics and depositional environment of Coleroon river sediments, Tamil Nadu, Southeast coast of India. *Journal of Coastal Sciences* 3(2):1-7 (2016).
46. M. Mehmood, A.A. Naseem, M. Saleem, J.U. Rehman, G. Kontakiotis, H.T. Janjuhah, and S.M. Siyar. Sedimentary Facies, Architectural Elements, and Depositional Environments of the Maastrichtian Pab Formation in the Rakhi Gorge, Eastern Sulaiman Ranges, Pakistan. *Journal of Marine Science and Engineering* 11(4): 726 (2023).
47. K.M. Farrell, W.B. Harris, D.J. Mallinson, S.J. Culver, S.R. Riggs, J. Pierson, J.M. Self-Trail, and J.C. Lautier. Standardizing Texture and Facies Codes for a Process-Based Classification of Clastic Sediment and Rock. *Journal of Sedimentary Research* 82(6): 364-378 (2012).
48. C. Zou, L. Wang, S. Tao, L. Hou, and A.J. Van Loon. Debrite turbidite transitions in the Chang 6 Oil Member of the Yanchang Formation (Ordos Basin, China). In: The Ordos Basin. R. Yang and A.J. Van Loon (Eds.). *Elsevier* pp. 411-420 (2022).
49. E.E. Hiatt. Sedimentology and sequence stratigraphy in basin analysis and paleohydrologic studies. In: Fluids and Basin Evolution. K. Kyser (Ed.). *Mineralogical Association of Canada, Ottawa* pp.19-38 (2000).
50. X. Sun, E. Gomez-Rivas, D. Cruset, J. Alcalde, D. Muñoz-López, I. Cantarero, and A. Travé. Origin and distribution of calcite cements in a folded fluvial succession: The Puig-reig anticline (south-eastern Pyrenees). *Sedimentology* 69(5): 2319-2347 (2022).
51. E.F. McBride. Quartz cement in sandstones: A review. *Earth-Science Reviews* 26(1-3): 69-112 (1989).
52. H.G. Reading (Ed.). Sedimentary Environments: Processes, Facies, and Stratigraphy *Blackwell Science Ltd*. (1996).
53. S. Hossain, H. Shekhar, and N. Rahman. Facies and architectural element analysis of the Upper Bokabil Sandstone in the Bengal Basin. *Sedimentary Geology* 453: 106433 (2023).
54. M. Yoshida and Y. Hamano. Pangea breakup and northward drift of the Indian subcontinent reproduced by a numerical model of mantle convection. *Scientific Reports* 5(1): 8407 (2015).
55. Z.F.M. Burton, T. McHargue, C.H. Kremer, R.B. Bloch, J.T. Gooley, C. Jaikla, J. Harrington, and S.A. Graham. Peak Cenozoic warmth enabled deep-sea sand deposition. *Scientific Reports* 13(1): 1276 (2023).
56. M. Umar, H. Friis, A.S. Khan, G. Kelling, A.M. Kassi, M.A. Sabir, and M. Farooq. Sediment Composition and Provenance of the Pab Formation, Kirthar Fold Belt, Pakistan: Signatures of Hot Spot Volcanism, Source Area Weathering, and Paleogeography on the Western Passive Margin of the Indian Plate during the Late Cretaceous. *Arabian Journal for Science and Engineering 39*: 311-324 (2014).
57. A.H. Kazmi and M.Q. Jan. (Eds.) Geology and Tectonics of Pakistan. *Graphic Publisher*s (1997).
58. A.H. Kazmi and I.A. Abbasi (Eds.). Stratigraphy and Historical geology of Pakistan. *Department & National Centre of Excellence in Geology, Peshawar, Pakistan* (2008).
59. M. Paryal, M.H. Agheem, G. Hussain, M.A. Kalwar, M. Hussain, and H. Asghar. Petrography of upper Nari Formation, Gandri Jabal, Pakistan. *North American Academic Research* 3(5): 178-199 (2020).